Refinement of Nanoporous Cu by Polyvinylpyrrolidone and Photodegradation of Methyl Orange by Cu_2O Nanowires and Nanoporous Cu Photocatalysts

Zhuxu XU [1], Yun LI [2], Fengxiang QIN [2], Zhenhua DAN [1 *]

[1] *College of Materials Science and Engineering & Tech Institute for Advanced Materials, Nanjing Tech University, Nanjing 211816, China*
[2] *School of Materials Science and Engineering, Nanjing University of Science and Technology, Nanjing 210094, China*

http://doi.org/10.5755/j02.ms.35363

Received 17 October 2023; accepted 31 January 2024

Refinement of nanoporous Cu (NP Cu) by the addition of Polyvinylpyrrolidone (PVP) in HF solution during dealloying of $Ti_{40.6}Zr_{9.4}Cu_{40.6}Ni_{6.3}Sn_{3.1}$ amorphous ribbons and effect of the surface coverage of Cu_2O nanowires obtained by immersing NP Cu in dehydrated ethanol on the photodegradation of methyl orange (MO) pollutants were investigated. The sizes of pores and ligaments of NP Cu decrease significantly with the increase of PVP concentration in the dealloying solutions, accompanied by a drastic decrease in the surface diffusivity and the dislocation defect densities. The surface coverage of Cu_2O nanowires becomes higher with an increase of the PVP reagents. The Cu_2O nanowires@nanoporous Cu (Cu_2O@NP Cu) catalysts show excellent photocatalytic activity towards the degradation of MO under the sunlight due to the existence of large amounts of heterojunctions between Cu_2O nanowires and Cu ligaments in nanoscale.
Keywords: nanoporous Cu, Cu_2O nanowires, dealloying, suppressed diffusivity by PVP, photodegradation.

1. INTRODUCTION

Photodegradation is one of the novel methods to treat polluted wastewater. Semiconductor-based photocatalysts have attracted more and more attention because of their low cost and availability, such as TiO_2 [1, 2] and Cu_2O [3]. The broad band gap of TiO_2 (3.0 – 3.2 eV) limits their applications since they can be only activated by ultraviolet (UV) light [2]. The photocatalysts with narrow band gaps can be activated by the sunlight with lower irradiation energy and are possibly used in the conversion of the solar energy. Therefore, Cu_2O catalysts with a direct band gap of 2.2 eV, have the potential to serve as the photocatalyst in solar energy conversion [3], such as photocatalytic degradation of Azo dyes [4] and decomposition of water into O_2 and H_2 [5], and so on.

On the other hand, nanoporous metals exhibit promising applications in the fields of catalysis [6], sensors [7], actuators [8], and fuel cells [9], due to ultrahigh surface area and unique bi-continuous ligament-pore structures. Dealloying is an effective method for the fabrication of nanoporous metals by preferential dissolution of active elements and rearrangement of the inert elements to form the porous structure [10]. Many noble nanoporous Au [11], Pd [12], and Pt [13] with high catalytic activities have been reported. Many researchers have contributed to functionalizing low-cost nanoporous metals and their composites, such as NP Cu [14] and Fe [15]. Nanoporous structures with smaller pore sizes have been reported to exhibit a superior catalytic performance [16]. Therefore, many efforts have been contributed to clarify the refinement of NP Cu by adding the surface capping agents to manipulate the surface diffusion. PVP has been widely used as a capping or stabilizing reagent for manipulate the crystal growths of nanometer-sized particles [17, 18] because PVP chain-like molecules with large molar mass are selectively adsorbed on specific metal crystallographic planes, resulting in the anisotropic metal growth [19].

Nanoporous metals and their oxide composite compounds in nanoscale size show higher photocatalytic efficiency than their bulk phase counterparts for the degradation of inorganic and organic pollutants [5, 20 – 22]. The heterojunctions of Cu and Cu_2O are regarded to enhance the photocatalytic activity of Cu_2O-base semiconductors since Cu may act as a pathway for the transferring of photoelectrons and avoid the combination of electron-hole pairs [21, 22]. So far, Cu_2O can be synthesized by many various methods, such as chemical, hydrothermal, and electrochemical methods [23 – 28]. Among them, chemical synthesis based on the chemical solution phase is widely used owing to the advantages such as simple handling, high yield, and quality, and easy control [26 – 28]. Many conductive polymers have attracted many scholars in the field of photocatalysis due to their fine synthesis and controllable chemical structure and electronic properties [29 – 30]. Moreover, the microstructure and shape of Cu_2O nanostructure have a key influence on the photocatalytic performance.

Effects of the addition of PVP into the dealloying solution on the refinements and characteristics of NP Cu and the changing tendency of the surface coverage of Cu_2O nanowires on the NP Cu substrates in dehydrated ethanol are investigated. Finally, the photocatalytic activity of Cu_2O@NP Cu composites was analysed at ambient temperature for the degradation of MO azo dyes.

* Corresponding author. Tel.: +86-25-83587270.
E-mail: *zhenhuadan@njtech.edu.cn* (Z. Dan)

2. EXPERIMENTAL PROCEDURE

A quinary alloy with nominal compositions of $Ti_{40.6}Zr_{9.4}Cu_{40.6}Ni_{6.3}Sn_{3.1}$ was prepared by arc melting a mixture of pure Ti, Zr, Cu, Ni, and Sn with a purity higher than 99.99 % in an Ar atmosphere. The melt spinning methodology was used to fabricate amorphous $Ti_{40.6}Zr_{9.4}Cu_{40.6}Ni_{6.3}Sn_{3.1}$ ribbons with 20 μm in thickness and 1 mm in width. Amorphous $Ti_{40.6}Zr_{9.4}Cu_{40.6}Ni_{6.3}Sn_{3.1}$ ribbons were chemically dealloyed in 0.2 M HF with different content of added PVP (0, 0.1, 1, 10 g/L) with a molar weight of 55,000 g mol^{-1} (Sigma Aldrich Co.) at free corrosion condition at 313 K for 6 h. The Cu_2O nanowires on NP Cu were obtained by immersing the as-dealloyed $Ti_{40.6}Zr_{9.4}Cu_{40.6}Ni_{6.3}Sn_{3.1}$ amorphous ribbons in dehydrated ethanol for 3 days. Nanomeasurer® software was employed to collect the average diameters of nanowires over 125 nanowires present in the corresponding SEM morphology [10, 14].

X-ray diffraction (XRD, Bruker-AXS D8, Karlsruhe, Germany) was used to confirm the phase constitution of the as-spun $Ti_{40.6}Zr_{9.4}Cu_{40.6}Ni_{6.3}Sn_{3.1}$ ribbons and the dealloyed ribbons. The surface microstructures of the as-dealloyed ribbons and the morphology of Cu_2O nanowires were characterized by a field-emission scanning electron microscope (SEM/EDS, QUANTA FEG 250, Hillsboro, OR, USA) equipped with an energy dispersive X-ray spectroscopy (EDS). The microstructures of Cu_2O nanowires were observed by transmission electron microscope (TEM, FEI Tecnai 20). The elemental valent was analyzed by an X-ray photoelectron spectrometer (XPS, THERMO ESCALAB 250XI, Waltham, MA, USA) with monochromatized Al Kα excitation (hν = 1486.6 eV). Photodegradation experiments were carried out by mixing 15 mg Cu_2O@NP Cu loadings into 5 mL 20 mg/L MO solution, which was exposed to sunlight for 25 mins. The concentrations of MO solution were detected by UV-vis spectroscopy (THERMO EVOLUTION 220, Waltham, MA, USA).

3. RESULTS

3.1. Fabrication and characteristics of Cu_2O@NP Cu

XRD patterns of $Ti_{40.6}Zr_{9.4}Cu_{40.6}Ni_{6.3}Sn_{3.1}$ ribbons before and after dealloying in 0.2 M HF, 0.2 M HF + 0.1 g/L PVP, 1 g/L PVP, and 10 g/L PVP solutions displayed in Fig. 1. As presented in Fig. 1 a, a broad diffraction peak at 2θ of 41° appears, indicating that as-spun $Ti_{40.6}Zr_{9.4}Cu_{40.6}Ni_{6.3}Sn_{3.1}$ ribbons are in an amorphous state. As shown in Fig. 1 b – e, three diffraction peaks at 43.3°, 50.4°, and 74.1° are assigned as fcc Cu (111), (200) and (220) in the patterns of dealloyed ribbons (JCPDS card No.: 02-1225). A small peak at 36.6° rising from Cu_2O (111) is present, which might be formed on the surface during the process of dealloying. The residues after dealloying in the four solutions are composed of fcc Cu and trace Cu_2O. As illustrated in the inset of Fig. 1, the defect density of NP Cu deduced from XRD patterns decreases with the increase of PVP concentration.

The dislocation defect density can be calculated by the formula [31]:

$$\rho = \frac{\beta^2}{4.35b^2}, \quad (1)$$

where ρ is the dislocation defect density; β is the FWHM measured by XRD rocking curves and b is Burgers vector. The dislocation defect density is 2.41×10^{17} m^{-2} of dealloyed sample in 0.2 M HF solution. In comparison to that of the NP Cu formed in 0.2 M HF solution, the dislocation defect density decreases to 3.23×10^{16} m^{-2} for 0.1 g/L PVP addition, 1.39×10^{16} m^{-2} for 1 g/L PVP addition and 1.35×10^{16} m^{-2} for 10 g/L PVP addition. In the previous work, it was found that Cu_2O nanostructure is preferentially to nucleate at the sites of defects such as twin boundaries [14]. Here, amorphous precursor alloys are favorable for the formation of the 2D Cu_2O architectures [14]. The concentration of HF solution and PVP capping agents might affect synergistically the surface area of the Cu ligaments and dislocation defect density in the Cu ligaments. Furthermore, the difference in dislocation defect density in the ligaments may play an important role in the subsequent growth of Cu_2O nanowires in dehydrated ethanol.

The surface morphology and corresponding distribution ratio of the nanopore and ligament sizes of the $Ti_{40.6}Zr_{9.4}Cu_{40.6}Ni_{6.3}Sn_{3.1}$ ribbons dealloyed in 0.2 M HF, 0.2 M HF+0.1 g/L PVP, 0.2 M HF+1 g/L PVP and 0.2 M HF+10 g/L PVP solutions for 6 h are presented in Fig. 2 and Fig. 3. The NP Cu formed on $Ti_{40.6}Zr_{9.4}Cu_{40.6}Ni_{6.3}Sn_{3.1}$ ribbons after dealloyed in 0.2 M HF solution exhibit a characteristics of mean pore size of 88 nm and ligament size of 110 nm. In comparison to the NP Cu formed in the 0.2 M HF solution, the sizes of pores and ligaments decrease to 50 nm and 65 nm in the solution with 0.1 g/L PVP addition, 38 nm and 40 nm in the solution with 1 g/L PVP addition, 25 nm and 28 nm in the solution with 10 g/L PVP addition. The pore sizes decrease obviously with PVP addition, illustrating that PVP macromolecules in the dealloying solution are effective in refining NP Cu. The PVP molecules exhibit an obvious effect on refining NP Cu with the increasing of their concentration, which is considered to result from the adsorption of the linear-chained PVP macromolecules onto the NP Cu and the suppression of the free diffusion of Cu adatoms.

3.2. Effect of PVP on surface diffusivity of Cu adatoms

According to the mechanism of surface diffusion controlled coarsening, The surface diffusivity (D_s) of Cu adatoms in different dealloying solutions can be estimated by the following equation [32]:

$$D_S = \frac{(d(t))^4 kT}{32\gamma t\alpha^4}, \quad (2)$$

where k is Boltzmann constant (1.3806×10^{-23} J/K); γ is surface energy of 1.79 J m^{-2} for Cu [33], t is the dealloying time; $d(t)$ is the mean pore size at the dealloying time t; T is the temperature, and α is the lattice constant.

Surface diffusivity of amorphous $Ti_{40.6}Zr_{9.4}Cu_{40.6}Ni_{6.3}$-$Sn_{3.1}$ ribbons after dealloying for 6 h was estimated to be 122.69×10^{-19} m^2s^{-1} in 0.2 M HF solution, 12.77×10^{-19} m^2s^{-1} in 0.2 M HF+0.1 g/L PVP solution, 4.25×10^{-19} m^2s^{-1} in

0.2 M HF+1 g/L PVP solution, and 0.81×10^{-19} m^2s^{-1} in 0.2 M HF+10 g/L PVP solution.

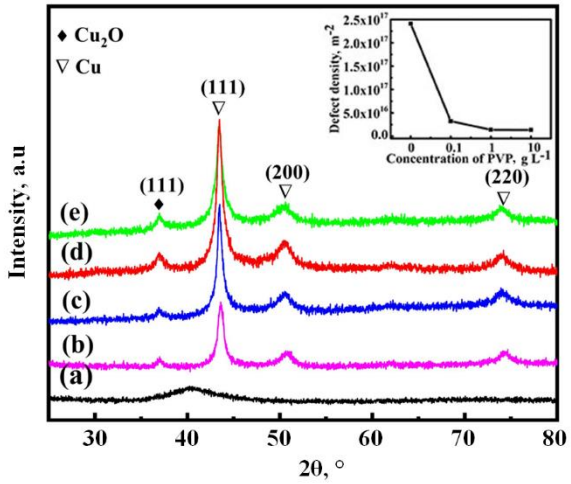

Fig. 1. XRD patterns of $Ti_{40.6}Zr_{9.4}Cu_{40.6}Ni_{6.3}Sn_{3.1}$ amorphous alloys: a – before dealloying for 6 h in 0.2 M HF; b – after dealloying for 6 h in 0.2 M HF; c – 0.2 M HF+0.1 g/L PVP; d – 0.2 M HF+1 g/L PVPl e – 0.2 M HF+10 g/L PVP (e) solutions. The inset is the dislocation defect density of the dealloyed alloys for the concentration of PVP

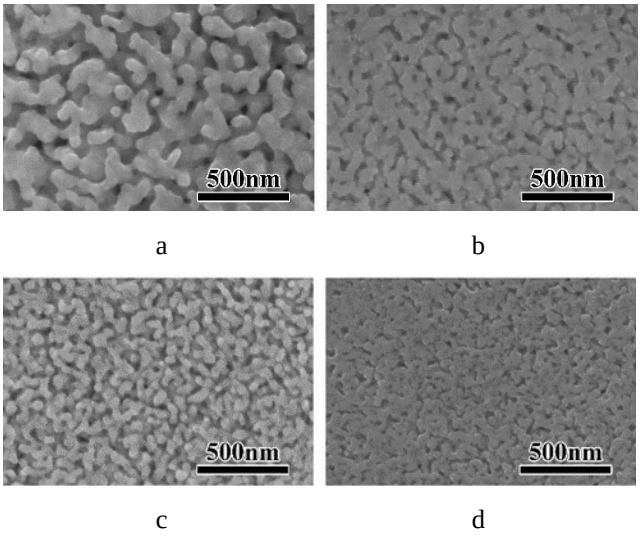

Fig. 2. SEM images of $Ti_{40.6}Zr_{9.4}Cu_{40.6}Ni_{6.3}Sn_{3.1}$ ribbons after dealloying for 6 h at 313 K under free corrosion condition in: a – 0.2 M HF, b – 0.2 M HF+0.1 g/L PVP; c – 0.2 M HF+1 g/L PVP; d – 0.2 M HF+10 g/L PVP solutions

The difference in D_s implies that the PVP macromolecules in the HF solution suppressed the surface diffusion of Cu adatoms by more than three orders of magnitude when the content of the PVP increased to 10 g/L. This phenomenon can be ascribed to the shorter-range diffusion instead of the free diffusion of Cu adatoms due to the adsorption of PVP macromolecules [19, 34]. The long range diffusion of the Cu adatoms at the metal/solution interface is suppressed due to the adsorption of PVP macromolecule chains [19, 34], resulting in finer nanopores in the PVP-added solutions.

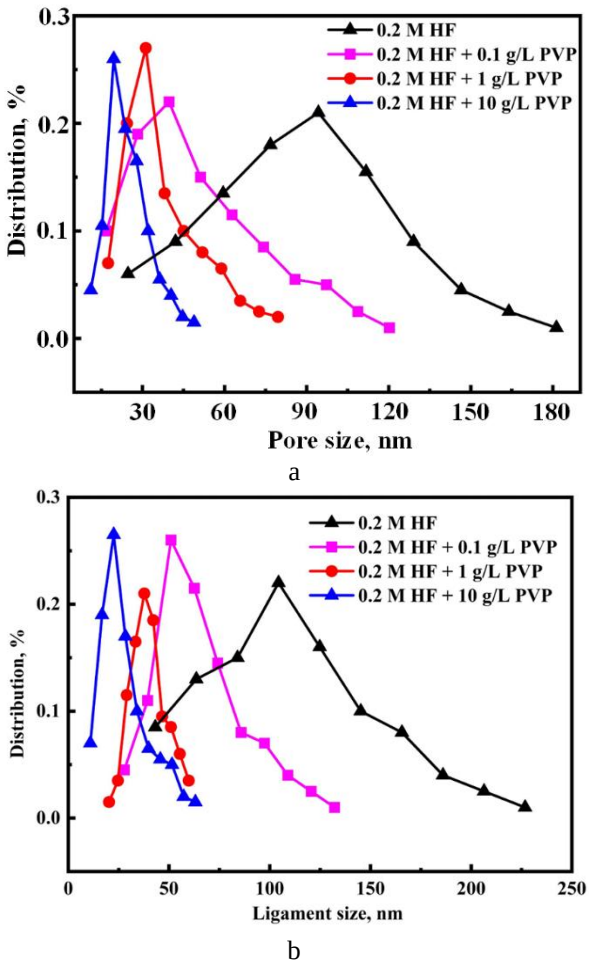

Fig. 3. The distribution ratios of: a – pore size; b – ligament size of as-dealloyed $Ti_{40.6}Zr_{9.4}Cu_{40.6}Ni_{6.3}Sn_{3.1}$ ribbons in different dealloying solutions

3.3. Morphology and photocatalytic activity of Cu_2O@NP Cu heterojunction photocatalysts

Fig. 4 demonstrates the surface morphologies of NP Cu after immersing in dehydrated ethanol for 3 days.

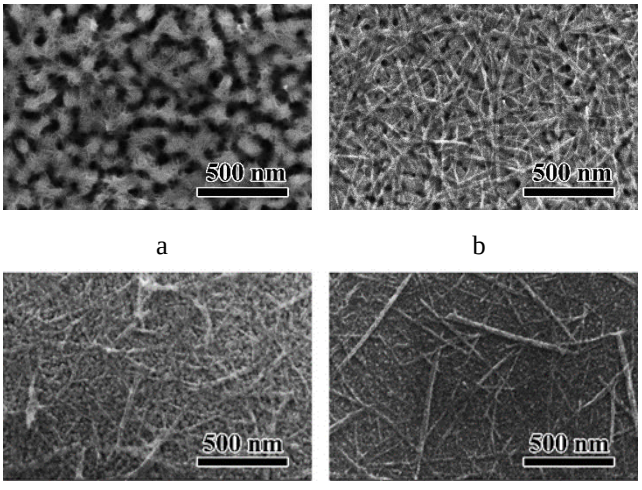

Fig. 4. SEM images of Cu_2O nanowires formed on the NP Cu substrates: a – after dealloying in 0.2 M HF; b – 0.2 M HF+0.1 g/L PVP; c – 0.2 M HF+1g/L PVP; d – 0.2 M HF+10 g/L PVP solutions and following immersion in dehydrated ethanol for 3 days at 298 K

A large number of belt-shape species are formed and covered partially on NP Cu. The growth and distribution of Cu_2O nanowires in Fig. 4 are several nanometers to several ten nanometers in width and several hundred nanometers in length, which are dependent on the initial pore structures of NP Cu with mean pore size ranging from 88 nm to 20 nm. The coverage fraction of Cu_2O nanowires increases with the increasing of pore sizes of the NP Cu substrates in Fig. 5, accompanying with decreasing in the width of Cu_2O nanowires. The ratio of surface coverage of Cu_2O nanowires are 40.4 %, 49.1 %, 72.6 % and 87.9 %, respectively, corresponding to the NP Cu with pore size from 25 nm to 88 nm. At the same time, with the increase in the width of Cu_2O nanowires, the less Cu_2O nanowires are formed on the surface of the NP Cu. The width of Cu_2O nanowires is wider and the coverage fraction of Cu_2O nanowires cut down, which might induce the photogenerated electrons and holes transfer to the Cu_2O surface more slowly in the electric field, although the conductive Cu ligaments help prompt photoelectrons transferring, which avoids the recombination significantly. However photocatalytic efficiency might decrease significantly with the increasing of the width of Cu_2O nanowires.

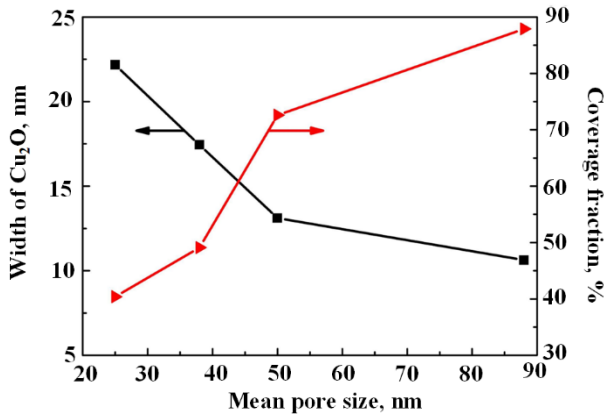

Fig. 5. Dependencies of width, coverage fraction of Cu_2O nanowires on the mean pore size of NP Cu substrates

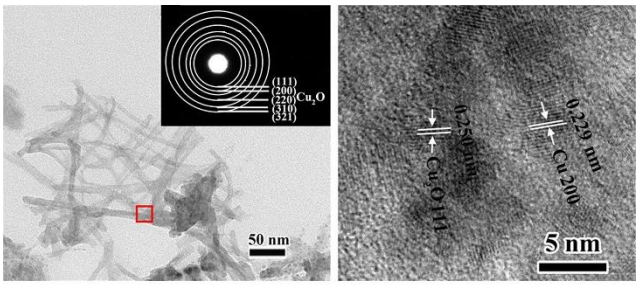

a b

Fig. 6. Bright-field TEM image of Cu_2O nanowires by immersing NP Cu in dehydrated ethanol for 3 days: a – selective area diffraction pattern; b – HRTEM image of the marked area in a

Fig. 6 a is the TEM image of the Cu_2O nanowires formed on the NP Cu substrate with a size of 88 nm by immersing NP Cu in dehydrated ethanol for 3 days. As has been seen, the Cu_2O nanowires are several hundred nanometers length in size growing from some sites in dark contrast, which might be NP Cu substrate. The selective area diffraction pattern of the marked position in Fig. 6 a, as shown in Fig. 6 b, is composed of several rings identified as (111), (200), (220), (310), and (321) crystal planes of Cu_2O, as well as (220) crystal plane of Cu, demonstrating the formation of Cu_2O on NP Cu. The interplanar distance from the adjacent lattice fringes of 0.250 nm corresponds to the (111) crystal plane of Cu_2O and 0.229 nm is identified as the (200) crystal plane of Cu in the HRTEM image in Fig. 6 c. According to the surface and interfacial effects of nanomaterials, the surface of NP Cu with high activity and strong adsorption, reacts directly with OH^- or dissolved oxygen in the solution. When NP Cu is immersed in dehydrated ethanol, the adsorption of OH^- ions on NP Cu from a small amount of H_2O molecules or dissolved oxygen in dehydrated ethanol helps to form the Cu_2O nanowires.

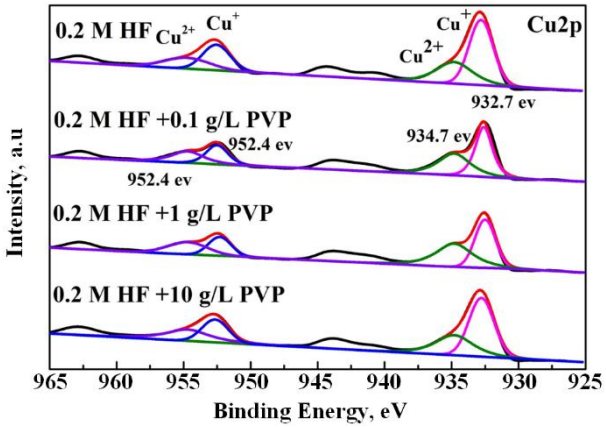

Fig. 7. XPS spectra of the Cu2p of the dealloying ribbons after immersion in dehydrated ethanol for 3 days

The XPS spectra of Cu in the Cu_2O nanowires of the dealloying ribbons after immersion in dehydrated ethanol for 3 days are shown in Fig. 7. The Cu2p spectra are composed of Cu_{2p3} and Cu_{2p1} peaks as well as the satellite peak. Cu_{2p3} peak is separated by two subpeaks at 932.7 and 934.7 eV, and Cu_{2p1} is constituted by two subpeaks at 952.4 and 954.8 eV, which are assigned to Cu^+ and Cu^{2+}. The appearance of a satellite peak indicates the existence of the oxidation state of Cu compounds due to the different binding energies of the photoelectrons from metallic states [35].

To evaluate the effect of the surface coverage of Cu_2O nanowires on the MO photodegradation of the Cu_2O@NP Cu catalysts, the UV-vis spectra of MO solution with the presence of the Cu_2O@NP Cu catalysts under irradiation of visible light for 25 min are measured. UV-vis spectra of MO solution degraded by Cu_2O@NP Cu catalysts with different coverages are illustrated in Fig. 8. The maximum absorbance peaks decay as the increase of coverage of Cu_2O nanowires on NP Cu substrate. The degradation efficiencies of MO increase gradually with the increasing of the coverage fraction of Cu_2O nanowires on NP Cu. When the coverage of Cu_2O increases from 40.4 % to 49.1 %, 72.6 %, and 87.9 %, the degradation efficiencies of MO solution degraded by Cu_2O@NP Cu catalysts enhance gradually from 87.8 % to 98.2 %. Fig. 8 b displays the relationship between degradation efficiency and the coverage fraction of Cu_2O nanowires. The degradation efficiency is linearly related to the coverage fraction of Cu_2O nanowires with a

correlation coefficient of 0.96. In other words, the more content of Cu_2O nanowires, the better the photocatalytic efficiency of the Cu_2O@NP Cu to MO solution can be obtained.

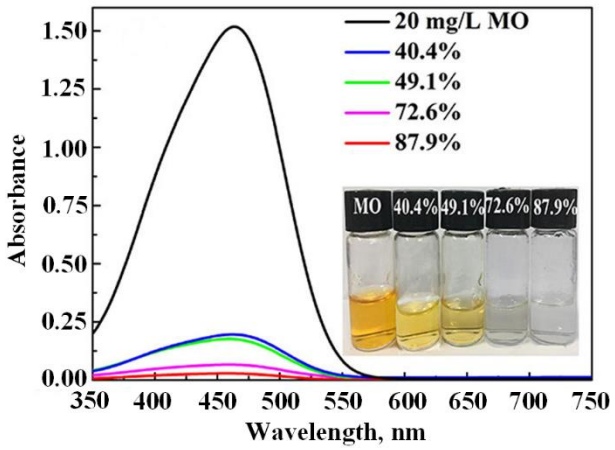

a

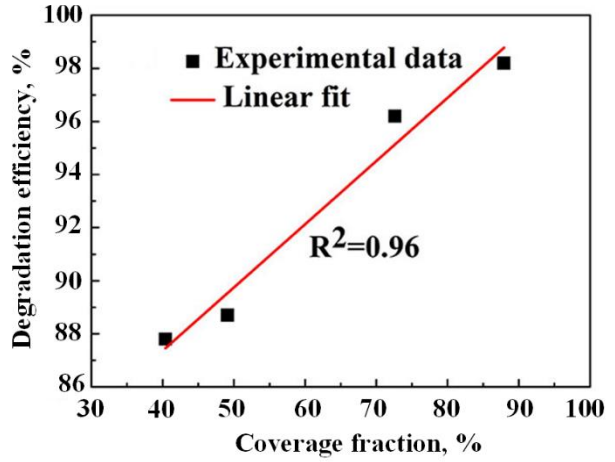

b

Fig. 8. UV-Vis absorbance spectra of the 20 mg/L MO solution degraded by Cu_2O@ NP Cu catalysts with different coverage fractions of Cu_2O nanowires for 25 min under irradiation of visible light.

4. DISCUSSION

A novel 2D-growth Cu_2O nanoarchitecture by simple chemical treatment of NP Cu in dehydrated ethanol proposed previously by our group can be extended and optimized [14]. The formation and final morphology of Cu_2O might be related to the pore sizes and the distribution of nanopores of Cu substrate and illustrate the relationship between the formation of Cu_2O architecture and characteristics of NP Cu substrate since the morphology of Cu_2O might affect the catalytic performance. Refinement of NP Cu by PVP acting as a stabilizing agent of the surface diffusion of Cu adatoms might be explained by the following: 1) Lessen the active sites of preferential dissolution during dealloying due to the adsorption of PVP macromolecules; 2) Restrict the free long-range diffusion of Cu adatoms by PVP macromolecules with a long chain. Based on the data in Fig. 3, more PVP macromolecules are added to the solution, the finer nanopores will form. Macroscopically, the adsorption of PVP macro molecules on the porous Cu surface reduces the surface active sites for the further selective dissolution of Ti atoms attacked by F^- anions. The positive dependence of the pore sizes and defect densities on the PVP concentration (Fig. 1 and Fig. 3 b) is attributed to the increasing adsorption of the PVP macromolecules on NP Cu. In the presence of PVP, NP Cu is stabilized and does not aggregate in size, because many C-O bonded sites multiply coordinate with the nanoporous surface [14, 19]. From the aspect of atomic scale, the long-chain PVP macromolecules, much larger than the Cu adatoms in the length direction, become the barrier for the movements of the Cu adatoms. Then the diffusion of Cu adatoms is suppressed by the PVP chains and the blocked Cu adatoms are forced to unite with the adjacent Cu adatoms to form both Cu clusters and Cu ligaments. Consequently, the diffusion and rearrangement of Cu adatoms were retarded significantly (Fig. 2) and the formation of smaller pores and narrower ligaments (Fig. 3). In other words, the existence of the adsorbed PVP chains restricts the free diffusion of the Cu adatoms in long range. The reducing extent of the porosity is governed by the PVP contents. Thereby, the surface diffusivity declines from 122.69×10^{-19} m^2s^{-1} in HF without PVP to 0.81×10^{-19} m^2s^{-1} in HF with 10 g/L PVP, which is fulfilled for the finer NP Cu.

On one hand, Cu_2O photocatalysts with different structures, such as nanocubes [36], nanocellular [37], nanodendrites [38], etc., have superior activities. The shape and the amount of the present Cu_2O nanowires have been controlled successfully through modifying the dealloying solutions by PVP addition. Ultrathin Cu_2O nanowires in Fig. 3 and Fig. 4 are formed on the NP Cu substrates. Cu_2O nanowires grew wider and longer on the NP Cu substrates with finer pores (Fig. 4), which formed on the NP Cu obtained in the more PVP-containing solution. Cu_2O nanowires in larger size are preferentially to grow on nanoporous structures with finer pores and ligaments, which might be linked with the different distribution of defects in different nanoporous substrates in Fig. 1. It is predicted that Cu_2O species nucleate at the active sites of defects in the nanoporous structure which are formed during the dealloying and pileup of the Cu adatoms [14, 19]. The ionized Cu adatoms at the tip of the defects, diffuse predominately by local transportation on the scale of the ligament length rather than by long-range transport to the outer surface [9, 14, 25, 27]. The ionized Cu adatoms are combined with OH^- or O^2 in the dehydrated ethanol to form Cu_2O species. Subsequently, part of Cu^+ is further oxidized to Cu^{2+}, and some of Cu^{2+} is preferentially reduced to Cu^+. In the XPS spectrum of Cu2p in Fig. 7, the Cu2p electron separated by two peaks originating from Cu^+ and Cu^{2+} ions. Moreover, ethanol molecules limits the growth of Cu_2O nanowires [14, 19], so that the two-dimensional growth of Cu_2O clusters is prevailed to form the nanowires [14, 27]. Thereby, the width of the nanowires increases rapidly, while the thickness does not increase significantly.

On the other hand, the increase of the defect density with the increase of the ligament size results in the enhancement of the nucleation sites and the decrease of the atomic diffusion distance for the formation of Cu_2O nuclei. Accordingly, as mentioned above, a high coverage fraction for thinner Cu_2O nanowires of 87.9 % is obtained on the NP

Cu with larger ligaments dealloyed in 0.2 M HF solution. With the decrease of the defect density by the PVP addition, the coverage fraction for Cu_2O nanowires decreases gradually down to 40.4 %. With the coverage fraction increase from 40.4 % to 87.9 %, the degradation efficiency is improved from 87.8 % to 98.2 %. Refinement of NP Cu results in a drastic decrease in the defects in the ligaments, which causes the lower nucleation density and higher growth rates of Cu_2O clusters. As a result, the manipulation of the shapes and numbers of Cu_2O species during the oxidation of Cu atoms by dissolved oxygen or OH^- in dehydrated ethanol has been done via defects engineering. The p-type semiconductor Cu_2O will be excited to produce electrons and holes under the irradiation of sunlight [3, 32]. The photogenerated electrons and holes will trigger a series of photodegradation reactions. Cu_2O nanowires grown on the surface of NP Cu lead to the redistribution of photogenerated electrons and oxidative photogenerated holes, then the formation of superoxide anion ($\bullet O^2$) and hydroxyl radicals (•OH) [4, 39], which play an important role in MO photodegradation. Cu_2O nanowires root on NP Cu by forming interfacial Cu_2O/Cu heterojunctions [22, 39]. The numbers of heterojunctions between NP Cu substrates and Cu_2O nanowires are directly related to the morphology of the nanostructure and the coverage fraction of Cu_2O. With the increase of the coverage fraction of Cu_2O nanowires, the numbers of heterojunctions rise. On one hand, NP Cu serves as the flowing path for photoelectrons and holes, and on another hand, Cu_2O nanowires functionalize as narrow bandgap photocatalysts. The coexistence of Cu_2O and Cu on the nanoscale is beneficial to high photocatalytic activity from the heterojunction effect by effective separation of photogenerated electron-hole pairs [17, 22, 37, 39]. Consequently, the quantum efficiency and the photocatalytic activity of Cu_2O are enhanced.

5. CONCLUSIONS

The effects of introducing PVP macromolecules into HF solutions on the formation of the NP Cu dealloyed by amorphous $Ti_{40.6}Zr_{9.4}Cu_{40.6}Ni_{6.3}Sn_{3.1}$ ribbons were investigated. After dealloying in PVP-added and PVP-free 0.2 M HF solution, NP Cu substrates with different pore and ligament sizes were formed. The sizes of the nanopores and ligaments decreased from 88 nm and 110 nm to 25 nm and 35 nm with the contents of PVP increasing to 10 g/L, accompanied by the decrease of the surface diffusivity in three orders of magnitude. The added PVP macromolecular was used to adjust the defect density and the nucleation density of Cu_2O clusters. Cu_2O nanowires have been formed via immersion of NP Cu in dehydrated ethanol. Both OH^- from water molecule acting as a reservoir and the dehydrated ethanol molecule serving as stabilizing or capping reagent promoted the 2D growths, are responsible for the formation of two dimensional Cu_2O nanowires. The Cu_2O@NP Cu photocatalysts exhibit excellent photocatalytic activity towards the degradation of MO under the irradiation of the sunlight due to the existence of the large amounts of heterojunctions between Cu_2O nanowires and Cu ligaments, which are beneficial to inhibiting the recombination of photogenerated photoelectrons and holes.

Acknowledgments

This work is financially supported by the National Key Research and Development Program of China (No. 2022YFB3705500), the National Natural Science Foundation of China under Grant No. 52371157 and 52375343, and Open Project of Taihu Laboratory of Deep-Sea Technology Science (2022JBGS01005). This work is partially supported by Priority Academic Program Development of Jiangsu Higher Education Institution (PAPD).

REFERENCES

1. **Zheng, Y.H., Chen, C.Q., Zhan, Y.Y., Zhu, Y.J.** Luminescence and Photocatalytic Activity of ZnO Nanocrystals: Correlation between Structure and Property *Inorganic Chemistry* 46 (16) 2007: pp. 6675 – 6682. https://doi.org/10.1021/ic062394m.s003
2. **Wang, Q.Z., An, N., Shi, Y.B., Fan, J.F., Huang, H.H., Su, B.T.** The Enhanced Photocatalytic Activity of Zn^{2+}, Doped TiO_2, for Hydrogen Generation under Artificial Sunlight Irradiation Prepared by Sol-gel Method *Journal of Sol-Gel Science and Technology* 73 (2) 2015: pp. 341 – 349. https://doi.org/10.1007/s10971-014-3538-7
3. **Briskman, R.N.** A Study of Electrodeposited Cuprous Oxide Photovoltaic Cells *Solar Energy Materials and Solar Cells* 27 (4) 1992: pp. 361 – 368. https://doi.org/10.1016/0927-0248(92)90097-9
4. **Ramirez-Ortiz, J., Ogura, T., Medina-Valtierra, J., Acosta-Ortiz, S.E., Lara, V.H., Bosch, P., De los Reyes, J.A., Lara, V.H.** A Catalytic Application of Cu_2O and CuO Films Deposited over Fiberglass *Applied Surface Science* 174 (3) 2001: pp. 177 – 184. https://doi.org/10.1016/S0169-4332(00)00822-9
5. **Hara, M., Kondo, T., Komoda, M., Ikeda, S., Shinohara, K., Tanaka, A., Kondo, J.N., Domen, K.** Cu_2O as A Photocatalyst for Overall Water Splitting under Visible Light Irradiation *Chemical Communications* 3 (3) 1998: pp. 357 – 358. https://doi.org/10.1039/A707440I
6. **Bond, G.C., Thompson, D.T.** Catalysis by Gold *Catalysis Reviews* 41 (3 – 4) 1999: pp. 319 – 388. https://doi.org/10.1081/CR-100101171
7. **You, T.Y., Niwa, O., Chen, Z.L., Hayashi, K., Tomita, M., Hirono, S.** An Amperometric Detector Formed of Highly Dispersed Ni Nanoparticles Embedded in a Graphite-like Carbon Gilm Electrode for Sugar Determination *Analytical Chemistry* 75 (19) 2003: pp. 5191 – 5196. https://doi.org/10.1021/AC034204K
8. **Weissmüller, J., Viswanath, R.N., Kramer, D., Zimmer, P., Wuerschum, R., Gleiter, H.** Charge-induced Reversible Strain in a Metal *Science* 300 (5617) 2003: pp. 312 – 315. https://doi.org/10.1126/science.1081024
9. **Joo, S.H., Choi, S.J., Oh, I., Kwak, J., Liu, Z., Terasaki, O., Ryoo, R.** Ordered Nanoporous Arrays of Carbon Supporting High Dispersions of Platinum Nanoparticles *Nature* 412 2001: pp. 169 – 172. https://doi.org/10.1038/35084046
10. **Dan, Z.H., Qin, F.X., Makino, A., Sugawara Muto, Y.I., Hara, N.** Fabrication of Nanoporous Copper by Dealloying of Amorphous Ti-Cu-Ag Alloys *Journal of Alloys And Compounds* 586 (5) 2014: pp. S134 – S138. https://doi.org/10.1016/j.jallcom.2013.01.087

11. **Xu, C.X., Su, J.X., Xu, X.H., Liu, P.P., Zhao, H.J., Tian, F., Ding, Y.** Low Temperature CO Oxidation Over Unsupported Nanoporous Gold *Journal of the American Chemical Society* 129 (1) 2007: pp. 42 – 43. https://doi.org/10.1021/ja0675503
12. **Wang, X.G., Tang, B., Huang, X.B., Ma, Y., Zhang, Z.H.** High Activity of Novel Nanoporous Pd-Au Catalyst for Methanol Electro-Oxidation in Alkaline Media *Journal of Alloys And Compounds* 565 (28) 2013: pp. 120 – 126.
13. **Yi, Q.F., Huang, W., Liu, X.P., Xu, G.R., Zhou, Z.H., Chen, A.C.** Electroactivity of Titanium-Supported Nanoporous Pd-Pt Catalysts Towards Formic Acid Oxidation *Journal of Electroanalytical Chemistry* 619 (1) 2008: pp. 197 – 205. https://doi.org/10.1016/j.jelechem.2008.03.012
14. **Dan, Z.H., Lu, J.F., Li, F., Qin, F.X., Chang, H.** Ethanol-Mediated 2D Growth Cu_2O Nanoarchitectures on Nanoporous Cu Templates in Anhydrous Ethanol *Nanomaterials* 8 (1) 2018: pp. 18 – 31. https://doi.org/10.3390/nano8010018
15. **Weng, N., Wang, F., Qin, F.X., Tang, W.Y., Dan, Z.H.** Enhanced Azo-dyes Degradation Performance of Fe-Si-B-P Nanoporous Architecture *Materials* 10 (9) 2017: pp. 1001 – 1013. https://doi.org/10.3390/ma10091001
16. **Wang, S.S., Zhang, C., Li, H.Y., Liu, L.** Enhanced Electro-Catalytic Performance of Pd-based Amorphous Nanoporous Structure Synthesized by Dealloying $Pd_{32}Ni_{48}P_{20}$ Metallic glass *Intermetallics* 87 2017: pp. 6 – 12. https://doi.org/10.1016/j.intermet.2017.04.002
17. **Tsuyama, H., Sakurai, H., Ichikuni, N., Negeshi, Y., Tsukuda, T.** Colloidal Gold Nanoparticles as Catalyst for Carbon-carbon Bond Formation: Application to Aerobic Homocoupling of Phenylboronic Acid in Water *Langmuir* 20 (26) 2004: pp. 11293 – 11296. https://doi.org/10.1021/la0478189
18. **Zhang, J.H., Liu, H.Y., Wang, Z.L., Ming, N.B.** Shape-Selective Synthesis of Gold Nanoparticles with Controlled Sizes, Shapes, and Plasmon Resonances *Applied Physics Letters* 17 (16) 2007: pp. 3295 – 3303. https://doi.org/10.1002/adfm.200700497
19. **Dan, Z.H., Qin, F.X., Hara, N.** Polyvinylpyrrolidone Macromolecules Function as a Diffusion Barrier During Dealloying *Materials Chemistry and Physics* 146 (3) 2014: pp. 277 – 282. https://doi.org/10.1016/j.matchemphys.2014.03.022
20. **Xu, L., Xu, H.Y., Wu, S.B., Zhang, X.Y.** Synergy Effect Over Electrodeposited Submicron Cu_2O Flms in Photocatalytic Degradation of Methylene Blue *Applied Surface Science* 258 2012: pp. 4934 – 4938. https://doi.org/10.1016/j.apsusc.2012.01.122
21. **Kou, T.Y., Wang, Y.Z., Zhang, C., Sun, J.Z., Zhang, Z.H.** Adsorption Behavior of Methyl Orange Onto Nanoporous Core-Shell $Cu@Cu_2O$ Nanocomposite *Chemical Engineering Journal* 223 2013: pp. 76 – 83. https://doi.org/10.1016/j.cej.2013.03.013
22. **Zhou, B., Liu, Z.G., Wang, H.X., Su, W.H.** Experimental Study on Photocatalytic Activity of Cu_2O/Cu Nanocomposites under Visible Light *Catalysis Letters* 132 (1 – 2) 2009: pp. 75 – 80. https://doi.org/10.1007/s10562-009-0063-3
23. **Song, H.C., Cho, Y.S., Huh, Y.D.** Morphology-Controlled Synthesis of Cu_2O Micro-Crystal *Materials Letters* 262 (10 – 11) 2008: pp. 1734 – 1736. https://doi.org/10.1016/j.matlet.2007.09.074
24. **Qu, Y.L., Li, X.Y., Chen, G.H., Zhang, H.J., Chen, Y.Y.** Synthesis of Cu_2O Nano-Whiskers by a Novel Wet-Chemical Route *Materials Letters* 62 (6 – 7) 2008: pp. 886 – 888. https://doi.org/10.1016/j.matlet.2007.07.004
25. **Zheng, J.Y., Jadhav, A.P., Song, G., Chang, W.K., Kang, Y.S.** Cu and Cu_2O Films with Semi-Spherical Particles Grown by Electrochemical Deposition *Thin Solid Films* 524 (12) 2012: pp. 50 – 56. https://doi.org/10.1016/J.TSF.2012.09.045
26. **Ram, S., Mitra, C.** Formation of Stable Cu_2O Nanocrystals in a New Orthorhombic Crystal Structure *Materials Science and Engineering A* 304 – 306 (1) 2001: pp. 805 – 809. https://doi.org/10.1016/S0921-5093(00)01578-1
27. **Wang, D.B., Yu, D.B., Mo, M.S., Liu, X.M., Qian, Y.T.** Seed-Mediated Growth Approach to Shape-Controlled Synthesis of Cu_2O Particles *Journal of Colloid and Interface Science* 261 (2) 2003: pp. 565 – 568. https://doi.org/10.1016/S0021-9797(03)00110-3
28. **Ahmed, A., Gajbhiye, N.S., Joshi, A.G.** Shape Controlled Synthesis and Characterization of Cu_2O Nanostructures Assisted by Composite Surfactants System *Materials Chemistry and Physics* 129 (3) 2011: pp. 740 – 745. https://doi.org/10.1016/j.matchemphys.2011.04.042
29. **Xua, Y.F., Mao, N., Zhang, C., Wang, X., Zeng, J.H., Chen, Y., Wang, F., Jiang, J.X.** Rational Design of Donor-π-Acceptor Conjugated Microporous Polymers for Photocatalytic Hydrogen Production *Applied Catalysis B: Environmental* 228 2018: pp. 1 – 9. https://doi.org/10.1016/j.apcatb.2018.01.073
30. **Xu, Y.H., Jin, S.B., Xu, H., Nagai, A., Jiang, D.L.** Conjugated Microporous Polymers: Design, Synthesis and Application *Chemical Society Reviews* 42 2013: pp. 8012 – 8031. https://doi.org/10.1039/C3CS60160A
31. **Xiong, J.J., Tang, J.J., Liang, T., Wang, Y., Xue, C.Y., Shi, W.L., Zhang, W.D.** Characterization of Crystal Lattice Constant and Dislocation Density of Crack-Free GaN Films Grown on Si(1 1 1) *Applied Surface Science* 257 2010: pp. 1161 – 1165. https://doi.org/10.1016/j.apsusc.2010.07.073
32. **Dona, J.M., Gonzalez-Velasco, J.** Mechanism of Surface Diffusion of Gold Adatoms in Contact with an Electrolytic Solution *The Journal of Physical Chemistry B* 97 (18) 1993: pp. 4714 – 4719. https://doi.org/10.1021/J100120A026
33. **Pluis, B., Frenkel, D., Veen, J.F.V.D.** Surface-Induced Melting and Freezing II.A Semi-Empirical Landau-Type Model *Surface Science* 239 (3) 1990: pp. 282 – 300. https://doi.org/10.1016/0039-6028(90)90231-V
34. **Dan, Z.H., Qin, F.X., Yamaura, S.I., Xie, G.Q., Makino, A., Hara, N.** Refinement of Nanoporous Copper by Dealloying MgCuY Amorphous Alloys in Sulfuric Acids Containing Polyvinylpyrrolidone *Journal of the Electrochemical Society* 161 (3) 2014: pp. C120 – C125. https://doi.org/10.1149/2.076403jes
35. **Chanquía, C.M., Sapag, K., Rodríguezcastellón, E., Herrero, E.R., Eimer, G.A.** Nature and Location of Copper Nanospecies in Mesoporous Molecular Sieves *The Journal of Physical Chemistry C* 114 (3) 2010: pp. 1481 – 1490. https://doi.org/10.1021/jp9094529
36. **Gou, L.F., Murphy, C.J.** Solution-Phase Synthesis of Cu_2O Nanocubes Nano Letters 3 (2) 2003: pp. 231 – 234. https://doi.org/10.1021/nl0258776
37. **Du, M., Zhang, H.W., Li, Y.X., Liu, Y., Chen, X., He, Y., Cheng, Y.** Fabrication of a Hierarchical Trimodal Structure

with Nano-Cellular Cu_2O, Nano-Porous Cu and Micro-porous Gasar Cu *Materials Letters* 164 (3) 2016: pp. 583 – 586. https://doi.org/10.1016/j.matlet.2015.11.024

38. **Niu, X.H., Pan, J.M., Qiu, F.X., Li, X., Yan, Y.S., Shi, L.B., Zhao, H.L., Lan, M.B.** Anneal-Shrinked Cu_2O Dendrites Grown on Porous Cu Foam as a Robust Interface for High-Performance Nonenzymatic Glucose Sensing *Talanta* 161 2016: pp. 615 – 622. https://doi.org/10.1016/j.talanta.2016.09.024

39. **Kou, T.Y., Jin, C.H., Zhang, C., Sun, J.Z., Zhang, Z.H.** Nanoporous Core-shell Cu@Cu_2O Nanocomposites with Superior Photocatalytic Properties towards the Degradation of Methyl Orange *RSC Advances* 2 (33) 2012: pp. 12636 – 12643. https://doi.org/10.1039/C2RA21821F